Applied Surface Science 504 (2020) 144336

Contents lists available at ScienceDirect

Applied Surface Science

journal homepage: www.elsevier.com/locate/apsusc

Full Length Article

On the catalytic role of superficial VO_x species and coke deposited on mesoporous MgO replica in oxidative dehydrogenation of ethylbenzene

Sebastian Jarczewski[a], Marek Drozdek[a], Piotr Michorczyk[b], Carlos Cuadrado-Collados[c], Jesus Gandara-Loe[c], Joaquín Silvestre-Albero[c], Lidia Lityńska-Dobrzyńska[d], Piotr Kuśtrowski[a,*]

[a] Department of Chemical Technology, Faculty of Chemistry, Jagiellonian University, Gronostajowa 2, 30-387 Kraków, Poland
[b] Institute of Organic Chemistry and Technology, Cracow University of Technology, Warszawska 24, 31-155 Kraków, Poland
[c] Laboratorio de Materiales Avanzados, Departamento de Química Inorgánica-Instituto Universitario de Materiales, Universidad de Alicante, Ctra. San Vicente-Alicante s/n, E-03690 San Vicente del Raspeig, Spain
[d] Institute of Metallurgy and Materials Science, Polish Academy of Sciences, Reymonta 25, 30-059 Kraków, Poland

ARTICLE INFO

Keywords:
Nanoreplication
Coke deposition
Magnesium vanadate
Regeneration
Oxidative dehydrogenation
Styrene production

ABSTRACT

Mesoporous MgO was synthesized by the nanoreplication method using CMK-3 carbon as a hard template and magnesium nitrate as a metal oxide precursor. The produced support was modified with different amounts of ammonium metavanadate solution. Various distributions of V-containing species on the MgO surface were found by XRD, low-temperature adsorption of N_2, TEM, XPS and UV–vis-DR spectroscopy. At low V loadings isolated VO_4 dominated. Increasing V content resulted in clustering of VO_4 species and the formation of $Mg_3V_2O_8$ crystallites. As found in temperature-programmed reduction (H_2-TPR), the latter phase was clearly harder in reduction by H_2 compared to highly dispersed VO_4 forms. The developed materials appeared to be very active catalysts of oxidative dehydrogenation of ethylbenzene (ODH). The optimal catalytic performance was observed for the sample containing 10 wt% of vanadium. The initial ethylbenzene conversion of 63.6% at selectivity to styrene of 86.9% was achieved at temperature as low as 500 °C. A notable influence of carbonaceous deposit formed during the ODH reaction on the catalytic activity was discussed, including presentation of both coexisting superficial reaction mechanisms. A reasonable regeneration procedure to recover lost activity was developed.

1. Introduction

Styrene is a very important monomer in the global polymer industry, due to a common application of various forms of polystyrene-containing homo- and copolymers. The main commercial technology of styrene manufacturing (> 80% of its worldwide production) is dehydrogenation of ethylbenzene over a promoted hematite catalyst in the presence of a substantial amount of superheated steam [1]. The process suffers due to reversible and endothermic nature of the dehydrogenation reaction, hence there is a strong incentive for the development of alternative technologies. In recent years much research has focused on oxidative dehydrogenation of ethylbenzene (ODH), because this approach exhibits significant benefits in contrast to the common dehydrogenation, i.e. exothermic heat effect and operation out of thermodynamic limitations [2]. Even though this technology was successfully implemented in the commercial butadiene manufacturing, no stable and selective enough system for the styrene production has been developed yet [3]. Among numerous transition metal oxides tested as catalysts in ODH, the vanadium-based ones (e.g. VO_x supported on γ-Al_2O_3 [4], SiO_2 [5] or MgO [6]) giving substantial ethylbenzene conversions (> 50%) and selectivities to styrene (> 90%) have attracted much attention. Hanuza et al. [7] proposed a redox mechanism of ODH involving vanadium active sites and oxygen bridges located in a V_2O_5/MgO system. From this point of view, the kind of metal oxide phase is a key factor for achieving an acceptable catalytic performance. Among studied V-Mg-O systems, magnesium orthovanadate ($Mg_3V_2O_8$) has been frequently reported as the active phase in ODH [8,9]. On the other hand, magnesium metavanadate and magnesium pyrovanadate were recognized to be responsible for total oxidation [10]. Surprisingly, bulk magnesium orthovanadate is significantly less active compared to supported systems, which are usually formed by an acid-base reaction of acidic vanadium oxide and basic MgO support [7,11]. Nevertheless, the optimal VO_x-MgO catalytic system configuration is still unrevealed.

One strategy to enhance the catalyst performance is to decrease

* Corresponding author.
E-mail address: piotr.kustrowski@uj.edu.pl (P. Kuśtrowski).

https://doi.org/10.1016/j.apsusc.2019.144336
Received 10 August 2019; Received in revised form 27 September 2019; Accepted 8 October 2019
Available online 23 October 2019

mass transfer limitations and as a consequence, to allow efficient diffusion of substrates toward active sites distributed inside the pores as well as easy evacuation of products from the pore system. For example, Pereira et al. [12] reported, that pores of very small dimensions are quickly blocked during the ODH process due to coke deposition, therefore rather mesoporous catalysts should be used. In 2005 Roggenbuck and co-workers [13] presented for the first time a synthesis of ordered mesoporous MgO, based on nanoreplication of 3D structure of hexagonal CMK-3 carbon rigid template. The presence of mesopores in this MgO support should provide similar advantages as in mesoporous carbon catalysts.

In this paper, we used mesoporous MgO synthesized by nanoreplication of sucrose-derived CMK-3 carbon template as a support for deposition of a vanadium precursor (NH_4VO_3). Different vanadium concentrations and calcination temperatures were studied in order to reveal the optimal surface properties responsible for fairly high catalytic activity in ODH. Accordingly, a comprehensive characterization of the obtained catalysts and a thorough discussion of the results of catalytic tests, including a possibility of simple regeneration and an influence of oxidizing agent content, are presented. To the best of our knowledge, this is the first attempt on the investigation of catalytic activity of ordered mesoporous VO_x-modified MgO replicas in the ODH reaction.

2. Experimental

2.1. Synthesis

Required CMK-3 carbon was prepared using SBA-15 as the hard template, and sucrose as the carbon precursor, which was carbonized at 850 °C, according to the procedure described earlier [14]. Corresponding X-ray powder diffraction patterns and low-temperature N_2 adsorption-desorption isotherms of the SBA-15 and CMK-3 materials are presented in Fig. S1 and Fig. S2, respectively. Mesoporous MgO replica was synthesized by the incipient wetness impregnation method. Briefly, 1.0 g of CMK-3 (initially dried at 120 °C for 12 h) was impregnated with 2.5 mL of 1.0 mol/L aqueous solution of magnesium nitrate ($Mg(NO_3)_2{\cdot}6H_2O$, POCH, p.a.) and dried in air overnight. The obtained composite was heated under a nitrogen atmosphere to 300 °C at a heating rate of 2.5 °C/min and kept at this temperature for 3 h, in order to convert magnesium nitrate to magnesium oxide within the pore system of the support. The procedure of impregnation and thermal treatment was repeated once, using a smaller volume of $Mg(NO_3)_2$ solution (2.0 mL/1 g of CMK-3). Finally, the carbon matrix was removed by heating the composite in air up to 750 °C at a heating rate of 2.5 °C/min and keeping the sample at the final temperature for 2 h. The obtained MgO replica is denoted as MG.

The V-Mg-O catalysts were synthesized by the wet impregnation method (using different volumes of solution containing a VO_x precursor) followed by complete evaporation of a solvent. In a typical procedure, 1.0 g of the previously synthesized MG sample (initially dried at 120 °C for 12 h) was immersed in a proper volume of 0.04 mol/L aqueous solution of ammonium metavanadate (NH_4VO_3, ACS reagent, ≥ 99%, Sigma-Aldrich). The volumes corresponded to an intended content of vanadium in the final catalyst, i.e. 2, 5, 10, 20 and 30 wt% of V, and were equal to 10.01, 25.81, 54.52, 122.69 and 210.34 mL, respectively. Each suspension was gently stirred with a magnetic stirrer at 60 °C until a paste was formed (ca. 1 h), subsequently transferred into an oven and dried at 60 °C for next 24 h in order to evaporate the solvent. After that time, the temperature was increased to 120 °C and kept for 48 h. Finally, the obtained powder was divided into two equal parts and each of them was calcined in air at 550 °C or 800 °C for 4 h at a heating rate of 1 °C/min. These temperatures were chosen based on thermogravimetric analyses of $Mg(NO_3)_2{\cdot}6H_2O$ and NH_4VO_3 (Figs. S3 and S4) as high enough to obtain vanadium-containing oxide phases, crucial from the catalytic point of view. The synthesized V-Mg-O catalysts are denoted as *x*VMG_*y*, where *x* is the intended vanadium concentration (wt%) and *y* is temperature of calcination.

For the comparison purposes, MgO was also synthesized by thermal decomposition of pure magnesium nitrate ($Mg(NO_3)_2{\cdot}6H_2O$, POCH, p.a.) in air at 350 °C for 3 h (a heating rate of 2.5 °C/min). Subsequently, the same procedure of wet impregnation with a NH_4VO_3 aqueous solution and calcination at 550 °C was employed in order to synthesize a reference sample containing 10 wt% of vanadium. The obtained material is denoted as 10VMGR_550.

2.2. Characterization methods

Powder X-ray diffraction (XRD) patterns of the synthesized CMK-3 and MgO replicas as well as V-Mg-O catalysts were collected with a Bruker D2 Phaser instrument using Cu Kα radiation (λ = 1.54184 Å) and a LYNXEYE detector in the 2θ range from 10.0 to 80.0° with a step of 0.02° and 1 s counting time per the step.

Textural parameters were investigated on the basis of low-temperature nitrogen adsorption–desorption isotherms collected at −196 °C using a Micromeritics ASAP 2020 sorptometer. Prior to each measurement, a sample was degassed in vacuum (10^{-3} Pa) at 250 °C for 6 h. Specific surface areas were calculated using the Brunauer–Emmett–Teller (BET) method. Values of total pore volume (V_{total}) were obtained from amounts of nitrogen adsorbed at relative pressure p/p_0 of 0.97. The equilibrium model of quenched solid density functional theory (QSDFT) was used to determine pore size distributions.

Temperature-programmed reduction (H_2-TPR) measurements were performed to evaluate the redox properties of the vanadium species. The experiments were carried out by heating 100 mg of a sample placed in a U-shaped microreactor from ambient temperature to 1000 °C (a heating rate of 10 °C/min) under a flow of H_2/He gas mixture (5/95 vol %, 25 mL/min). Prior to the experiment, the sample was heat treated in a helium flow (50 mL/min) at 200 °C for 2 h to remove moisture and impurities. Evolving H_2O and unreacted H_2 were analyzed quantitatively with an Omnistar Balzer MSC200 quadrupole mass spectrometer after calibration based on full reduction of CuO in the range of 25–700 °C.

Ultraviolet visible diffuse reflectance (UV–Vis-DR) spectra for powder samples were collected in air at ambient temperature in the range of 190–800 nm using a Thermo Scientific Evolution 220 spectrophotometer with resolution of 1 nm and counting time of 1.5 s/nm. Prior to the experiment, the samples were dried in air at 120 °C for 2 h.

Quantitative analyses of elements present in all oxide samples were performed with X-ray fluorescence spectroscopy (XRF) using a Thermo Scientific ARL Quant'x spectrometer.

A surface composition of samples was investigated with X-ray photoelectron spectroscopy (XPS) using a Prevac photoelectron spectrometer equipped with a hemispherical analyzer (VG SCIENTA R3000). The spectra were taken using a monochromatized aluminum source Al Kα (E = 1486.6 eV). The base pressure in the analytical chamber was 5×10^{-9} mbar. The scale of the binding energy value was adjusted to the C 1s reference peak at 284.8 eV. The composition and chemical state of sample surface were analyzed taking into account the areas and binding energies of O 1s, C 1s, V 2p and Mg 2p photoelectron peaks. The spectra were fitted using CasaXPS software.

Thermogravimetric analyses (TG) were performed with a SDT Q600 thermobalance (TA Instruments) in flowing air (100 mL/min) from 30 °C to 1000 °C (at a heating rate of 20 °C/min).

Transmission electron microscopy (TEM) was used to visualize morphology of the produced MgO support and V-Mg-O catalysts. The images were collected in a JEOL JEM-2010 microscope equipped with an Oxford Inca Energy TEM 100 detector and a Gatan Orius SC600 digital camera, operating at 200 kV. Prior to the experiments, samples were deposited on a copper grid with a carbon film support. The high resolution TEM micrographs were taken using a TEM FEI transmission

electron microscope Tecnai G2 operating at 200 kV equipped with a high-angle annular dark field scanning transmission electron microscopy detector (HAADF-STEM).

2.3. Catalytic tests

The synthesized V-Mg-O materials were tested as catalysts in the oxidative dehydrogenation of ethylbenzene (EB) to styrene in the presence of oxygen at the molar ratio of O_2:EB = 1:1, 2:1 and 3:1. The reaction was carried out in a packed bed flow microreactor with 50 mg of a sample placed onto a quartz wool plug. The temperature was measured with a thermocouple, protected by a quartz capillary inserted directly into a catalyst bed. The gaseous reactants were fed through mass flow controllers (Brooks 4800) at a total flow rate of 50 mL/min. Depending on the O_2:EB molar ratio, flows were set as follows: 0.4 mL/min O_2 and 49.6 mL/min He (1:1); 0.8 mL/min O_2 and 49.2 mL/min He (2:1); 1.2 mL/min O_2 and 48.8 mL/min He (3:1). The EB vapor was introduced into the flow of O_2/He mixture by passing it through a glass saturator filled with liquid EB and kept at 25 °C. The products of the reaction were sampled with a pneumatic valve and transferred into a gas chromatograph system (Bruker 450-GC) via a heated line. The gas chromatograph was equipped with three packed columns (Porapak Q, Molecular Sieve 5A and Chromosorb W-HP) connected with two flame ionization detectors (one of them directly connected to a catalytic methanizer) and one thermal conductivity detector. Prior to a catalytic run, a catalyst was outgassed at 200 °C in flowing He (50 mL/min) for 30 min. Subsequently, the temperature was increased to 500 °C and dosing of the reactants begun. After 15 min of time-on-stream (TOS), a first sample of outlet stream was injected to GC and the analysis started. The chromatographic analyses were performed in 42 min intervals within a total time of 7 h. The catalytic performance was evaluated in terms of the following parameters:

$$X_{EB} = ((F_{EB,0} - F_{EB})/(F_{EB,0})) \times 100\%$$

$$Y_i = (F_i/F_{EB,0}) \times 100\%$$

$$S_i = (Y_i/X_{EB}) \times 100\%$$

where X_{EB} – conversion of EB, $F_{EB,0}$ and F_{EB} – molar flow rate of EB in the inlet and outlet streams, Y_i – yield of i product, F_i – molar flow rate of EB transformed into i product, and S_i – selectivity of i product.

3. Results and discussion

3.1. Physicochemical properties of V-Mg-O catalysts

Morphology of mesoporous MgO before modification and the samples after the introduction of V-containing species was investigated by TEM. In the collected micrographs of the MG support (Fig. 1A and A′) domains with the 2D hexagonal pore arrangement, expected for an inverse replica of CMK-3 carbon template, are identified. Nevertheless, a long-range structural ordering of this sample is relatively low. The selected type of oxide precursor (namely magnesium nitrate) and peculiar conditions of its thermal decomposition caused that various gaseous oxidants (i.e. O_2 and NO_2) could be evolved inside the pores of the carbon template during the thermal treatment. Therefore, unavoidable partial oxidation of the carbon matrix by these oxidants, most probably occurred at elevated temperatures, since the assumed structure of silica template as well as carbon template was verified in advance (cf. Figs. S1 and S2). As a consequence, the perfect long-range ordering of the carbon template was partially lost after the first step of impregnation with the solution of magnesium nitrate. However, the obtained MG sample exhibited expected mesoporosity, confirmed by adsorption measurements (discussed further), and was used as a support of vanadium-based active phase.

The TEM picture of the catalyst with 10 wt% loading of vanadium (Fig. 1B) reveals highly dispersed particles of the $Mg_3V_2O_8$ phase (pointed with black arrows). It should be kept in mind, that also smaller domains of VO_x species can be present, which are not visible in the standard mode of TEM measurements. Therefore, high resolution TEM micrographs were taken (cf. Fig. S5A). Subsequently, the fast Fourier transform (FFT) was used to create the diffraction pattern with spots typical for crystalline phases (Fig. S5B). Based on the particular spots, the calculated interplanar spacings were equal to 0.286 nm and 0.211 nm. These values correspond accurately to interplanar spacings reported in the Powder Diffraction Files of International Centre for Diffraction Data (MgO, PDF 00-004-0829; $Mg_3V_2O_8$, PDF 00-037-0351) for the planes indexed as (0 4 0) for $Mg_3V_2O_8$ and (2 0 0) for MgO phases, respectively [15]. Interestingly, the value as high as 0.286 nm is not indexed for the MgO phase in the PDF data (0.243 nm is the highest value), and confirms the existence of $Mg_3V_2O_8$ phase on the surface of MgO support. Inverse FFT generated from the selected pattern spots correlated with $Mg_3V_2O_8$ provides a map of vanadium-containing phase (Fig. S5C).

Low-temperature nitrogen adsorption-desorption isotherms were collected for the magnesium oxide support and the vanadium-containing samples (Fig. 2) in order to determine their textural parameters (Table 1). A certain increase of adsorption effect within the whole p/p_0 range as well as a hysteresis loop (type H2(b) according to the IUPAC classification) [16] observed in the isotherm of MG informs us about non-uniformity of size and shape of pores of this material. The MG support exhibits a specific surface area of 167 m^2/g and a total pore volume of 0.46 cm^3/g, which confirm that the nanoreplication technique leads to the production of high-surface area magnesium oxide, as intended. On the contrary, magnesium oxide obtained for comparison by simple thermal decomposition of $Mg(NO_3)_2{\cdot}6H_2O$ (cf. Experimental section) shows surface area as low as 23 m^2/g and total pore volume of 0.05 cm^3/g.

After the insertion of vanadium species, the BET surface areas and total pore volumes of the resulting materials decrease compared to the parent MG. For the sample with the smallest V content (2VMG_550), the BET surface area drops to 48 m^2/g, which is presumably related to partial clogging narrow pores by a deposited vanadium-containing phase. This effect can be observed in the pore size distribution (Fig. S6). Namely, the bimodal distribution of the MG support was preserved after impregnation with the vanadium precursor, however the porosity and specific surface area decreased. On the other hand, a slight increase in the BET surface area is observed with the raising vanadium content probably due to the formation of porous vanadium-containing particles as well as modification of the pore structure of the MG support. The latter phenomenon is a result of hydration and subsequent dehydration of magnesium oxide caused by an aqueous solution used during wet impregnation. With the increasing intended vanadium content, the higher volumes of saturated solution of ammonium metavanadate entail longer impregnation times. Consequently, the MG support becomes more hydrated and shows tendency to the formation of additional porosity by dehydration during calcination [17]. This effect is also observed for the 10VMGR_550 sample, based on MgO synthesized by simple thermal decomposition of $Mg(NO_3)_2{\cdot}6H_2O$. The specific surface area and total pore volume raised up to 56 m^2/g and 0.20 cm^3/g, respectively. The low-temperature N_2 adsorption–desorption isotherm is depicted in Fig. S7. According to the IUPAC classification, an isotherm can be described as type IIB for macroporous solids [16]. Similar S_{BET} variations were reported by few authors not only for vanadium-based materials, but for other metal oxides as well. However, no consistent trends have been found in the literature, because either increase or decrease in a specific surface area is reported for various V-Mg-Si-O materials [17–27].

The phase composition of the MG and *x*VMG_550 catalysts, being a result of thermal-induced reaction between the MgO support and ammonium metavanadate, was examined with X-ray powder diffraction (Fig. 3A). For all vanadium-containing catalysts, the distinct peaks are

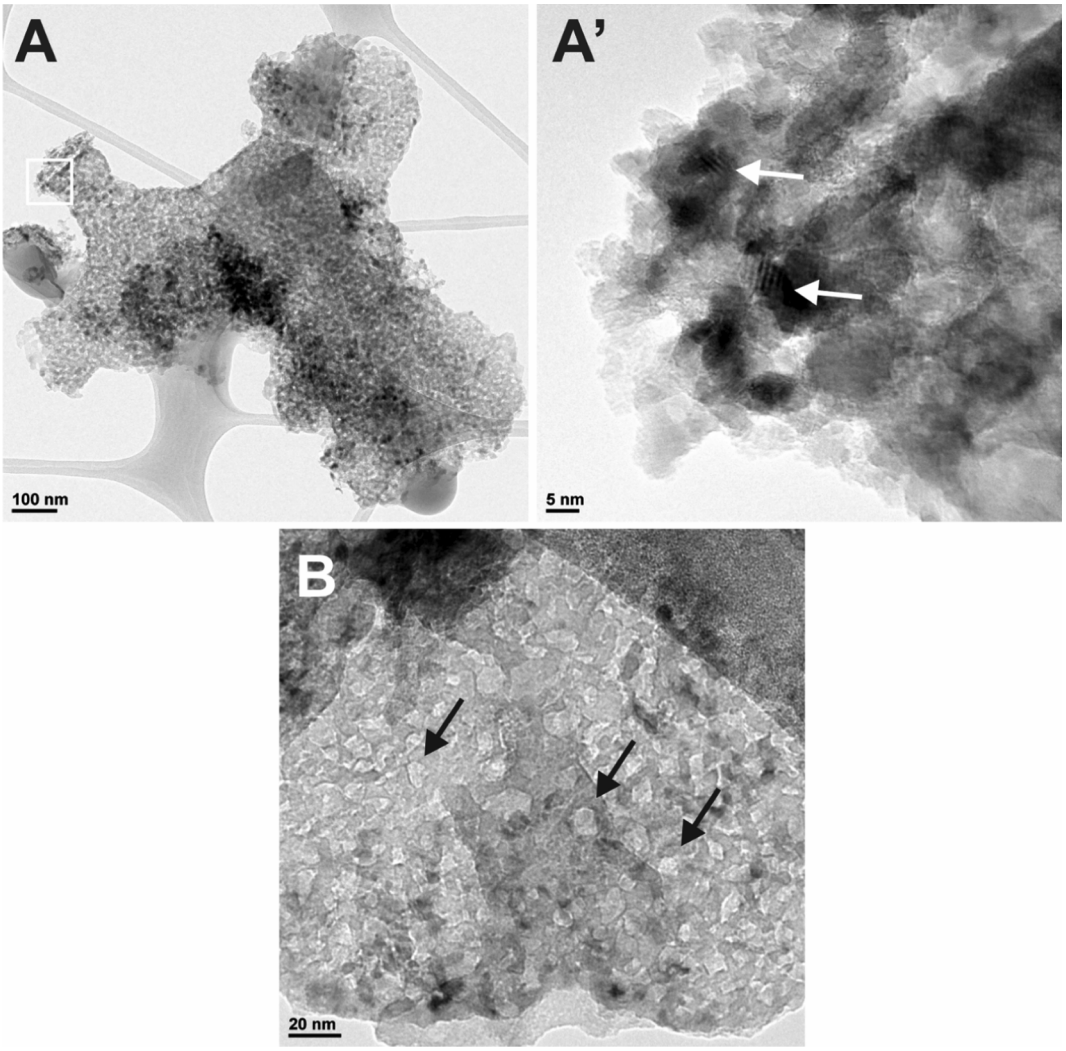

Fig. 1. TEM micrographs of MG support (with magnitude of 5×10^4 – A and 1×10^6 – A′) and 10VMG_550 sample (B).

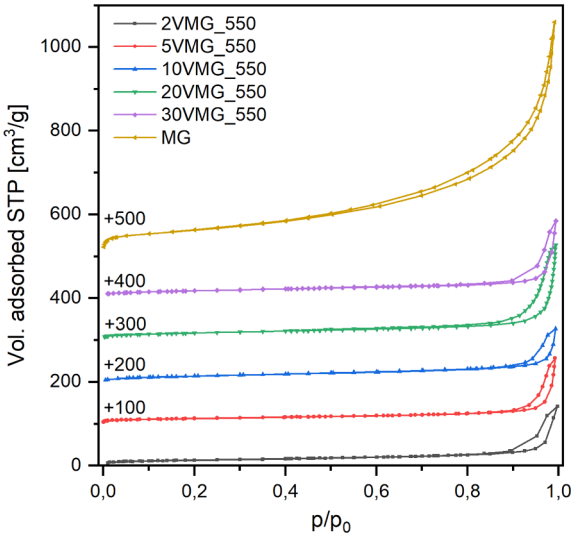

Fig. 2. Low-temperature nitrogen adsorption-desorption isotherms for MG and *x*VMG_550.

observed at the same positions as for the parent support. These diffraction lines are typical of the periclase phase (MgO, PDF 00-004-0829) [15]. Their intensities consistently decrease with the raising vanadium loading. On the other hand, for the samples with lower vanadium loadings (below 20 wt% of vanadium), the XRD peaks attributed to vanadium-containing phase(s) are not visible, possibly because of their high dispersion and relatively low dimensions of particles. The higher V loading results in the appearance of diffraction lines, especially at 30 and 36° 2θ, typical of magnesium orthovanadate ($Mg_3V_2O_8$, PDF 00-037-0351) [23,15,28]. No distinctly visible peaks typical of V_2O_5 are observed (the reference pattern of this phase including relative peak intensities is presented in Fig. 3B, PDF 00-041-1426). The

Table 1
Chemical composition, porosity and reducibility of the MG and *x*VMG_550 samples.

Catalyst	Vanadium content in bulk [wt. %][a]	Atomic V/Mg ratio		Textural parameters		H_2 consumption [mmol/g][c]	
		Bulk[a]	Surface[b]	S_{BET} [m^2/g]	V_{total} [cm^3/g]	low-*T* peak	high-*T* peak
MG	–	–	–	167	0.46	–	–
2VMG_550	2.3	0.04	0.02	48	0.22	0.24	0.48
5VMG_550	5.1	0.10	0.05	47	0.24	0.19	1.19
10VMG_550	9.6	0.20	0.09	53	0.39	0.14	2.17
20VMG_550	19.4	0.49	0.23	62	0.35	0.07	4.31
30VMG_550	30.5	0.96	0.29	64	0.29	0.04	6.46

[a] – XRF; [b] – XPS; [c] – TPR.

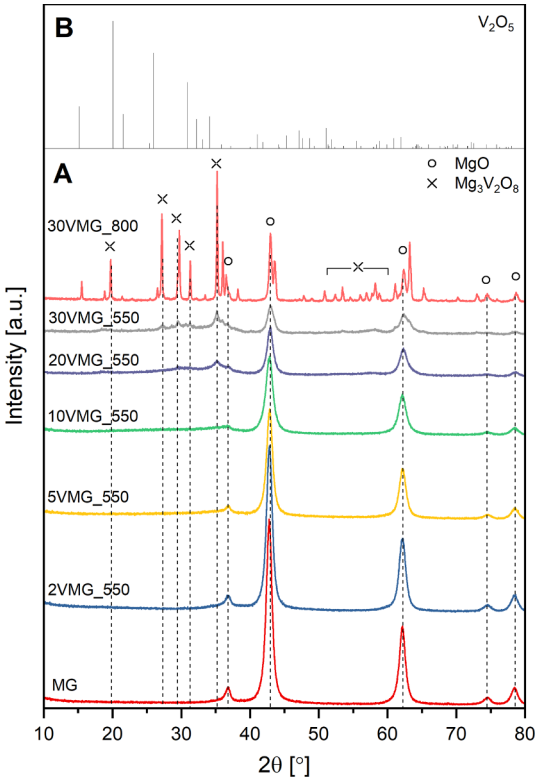

Fig. 3. XRD patterns of the MG support and *x*VMG catalysts calcined at 550 °C and 800 °C (A) and reference V_2O_5 (PDF 00-041-1426) (B).

size of $Mg_3V_2O_8$ crystallites calcined at 550 °C is rather small, but increases significantly after calcination at elevated temperature (compare the XRD pattern of 30VMG thermally treated at 800 °C presented in Fig. 3A). The mean crystallite size calculated from the Scherrer equation based on the FWHM of the (1 3 1) diffraction peak at 29.6° 2θ is 45.5 nm for 30VMG_800, and 9.5 nm for 30VMG_550 (thus nearly 5 times smaller).

It is worth to note, that diffraction peaks assigned to α-$Mg_2V_2O_7$ (magnesium pyrovanadate) were not detected. The α-$Mg_2V_2O_7$ phase is commonly considered as a transitional form during the formation of magnesium orthovanadate. Intriguingly, this finding proves, that $Mg_3V_2O_8$ can be formed at temperature as low as 550 °C, in contrast with results published previously by Oganowski et al. [9], who reported the crystallization of other vanadium-magnesium phases at this temperature.

In order to elucidate the oxidation state of vanadium on the surface of catalysts, X-ray photoelectron spectroscopy measurements were performed. The XPS V $2p_{3/2}$ spectra collected for the whole *x*VMG_550 series are presented in Fig. 4. For each sample, the peak corresponding to the photoelectron emission from the V $2p_{3/2}$ level is observed at the binding energy of 517.1 ± 0.2 eV. The symmetric shape of this peak without any shoulder at lower binding energies (especially at E_b = 516.3 eV, typical of V^{4+}) confirms that V^{5+} species exist exclusively on the sample's surface [29–31]. The area of the V $2p_{3/2}$ peak increases with the raising vanadium loading due to a progressive insertion of vanadium species. The superficial atomic V/Mg ratios (determined by XPS) are compared for all samples to the corresponding bulk V/Mg ratios (determined by XRF) in Table 1. It is observed, that the amounts of V on the surface are lower than those in the bulk, which in turn are very close to the assumed V concentrations.

The temperature-programmed reduction measurements were performed for the catalysts calcined at 550 °C, to give more specific information about reducibility of the V-containing active phase (Fig. 5). For all samples, two main peaks related to hydrogen consumption can

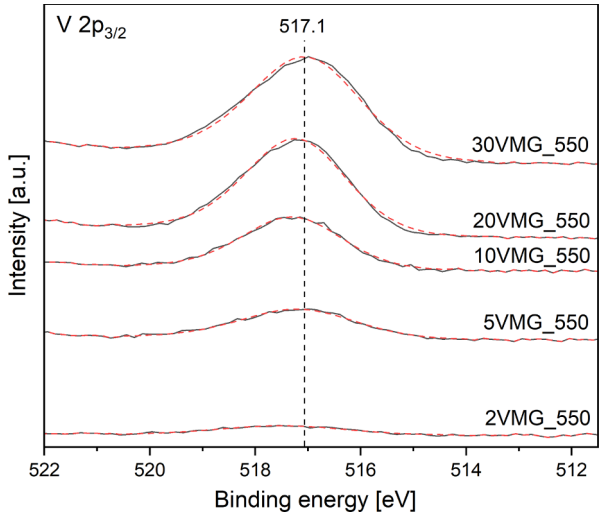

Fig. 4. XPS V $2p_{3/2}$ spectra collected for the *x*VMG_550 catalysts.

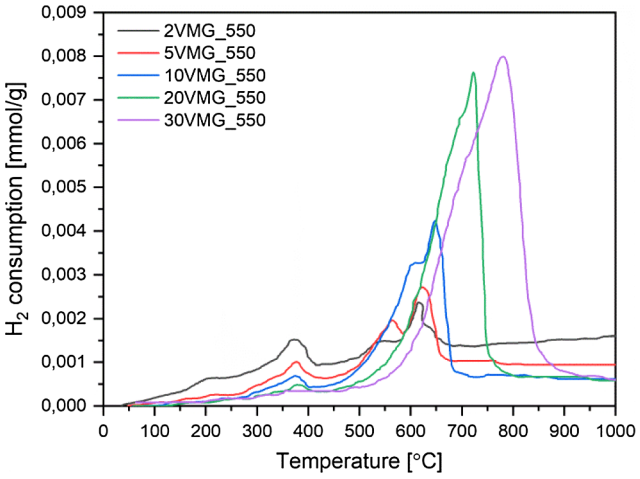

Fig. 5. H_2-TPR profiles of the *x*VMG_550 catalysts.

be found. Quantitative analysis of their areas related to the amount of H_2 consumed is summarized in Table 1. The first reduction peak is observed at ca. 375 °C. The area of this peak, which is related to reduction of V^{5+} in isolated VO_4 with tetrahedral coordination, decreases with the increasing vanadium loading. The second reduction peak observed at higher temperature consists of two components, attributed to reduction of V^{5+} ions located in larger domains of $Mg_3V_2O_8$. The low-*T* and high-*T* shoulder components can be assigned to the reduction of bidimensional and disordered 3D polymeric structures, respectively [23,32–35]. Interestingly, for the samples with 20 and 30 wt% of vanadium, the high-temperature peak shifts its position to significantly higher temperatures. Furthermore, its area increases with the raising vanadium loading. It should be therefore noticed, that the introduction of higher contents of V results in aggregation of tetrahedral VO_4 forms into larger crystallites of $Mg_3V_2O_8$, confirmed by the XRD results.

The form of vanadium species present on the surface of catalysts was also studied with UV–Vis-DR spectroscopy (Fig. 6A). For the samples with a low amount of vanadium (2–10 wt%), only one band is observed at 275–285 nm, which corresponds to charge transfer (CT) transition t_2 (oxygen) → e (vanadium V^{5+}) in isolated VO_4 tetrahedral forms. The intensity of this band increases with the raising vanadium loading and reaches the maximum value for 10VMG_550. At the higher vanadium loadings (20VMG_550 and 30VMG_550) the absorbance for this band decreases, but the new band appears at higher wavelengths (312 nm and 325 nm, respectively) [9,25,36]. This indicates the

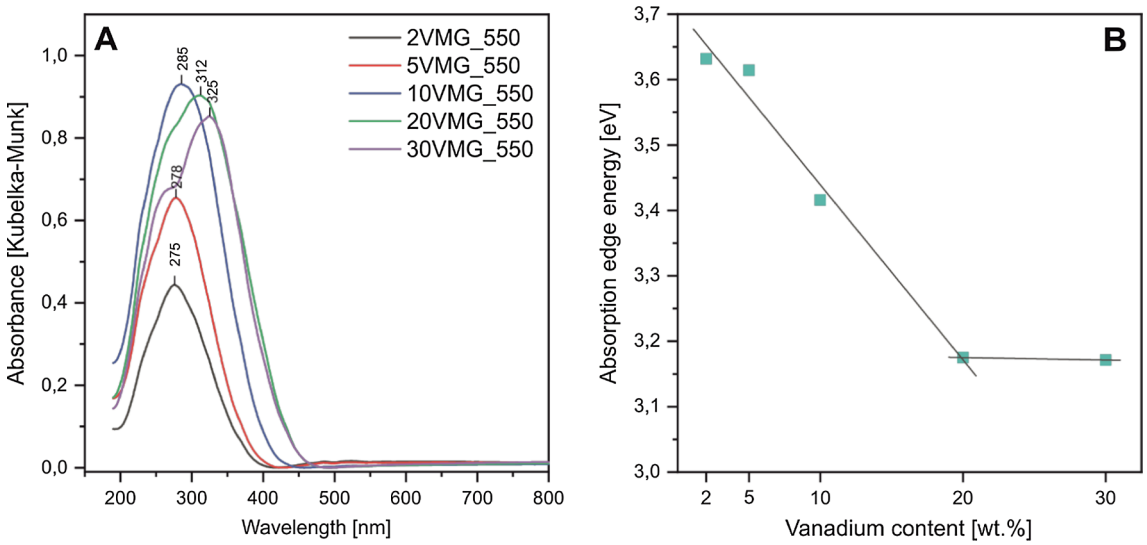

Fig. 6. UV–Vis-DR spectra (A) and calculated absorption edge energies (B) for the *x*VMG_550 catalysts.

increase in the vanadium coordination number and/or the formation of tetrahedral or octahedral oligomeric forms on the surface. Thus, the relative amount of isolated VO_4 decreases with the increasing vanadium loading, that corresponds with the H_2-TPR results. Moreover, the absence of band at 580–810 nm, attributed to the d-d transition for V^{4+}, confirms a dominant role of V^{5+} ions in the studied catalysts [36].

For all supported catalysts, absorption edge energy (E_g) was calculated (Fig. 6B), according to the procedure described by Weber et al. [37], to investigate more precisely the structure of surface active phase. The determined values (E_g = 3.15–3.65 eV) are close to that reported in the literature for magnesium orthovanadate in the form of isolated VO_4 species ($E_g \sim 3.4$ eV) [25,38–40]. In the reported region dimeric forms of magnesium pyrovanadate $Mg_2V_2O_7$ are located as well ($E_g \sim 3.2$ eV), however the presence of this phase was not confirmed by other techniques. On the other hand, E_g for two-dimensional forms of magnesium metavanadate MgV_2O_6 is in the range of 2.5–2.8 eV and for distorted tetragonal bipyramids V_2O_5 – ca. 2.2–2.4 eV, thus much lower than calculated for the synthesized catalysts [38,39]. The observed decrease in absorption edge energy with the increasing vanadium amount is related to growing the V-containing domains on the surface [25,37], which is consistent with the complementary results of the XRD and H_2-TPR measurements. Moreover, the lower absorption edge energy is a consequence of higher coordination number of central atom [38,40]. The 20VMG_550 and 30VMG_550 samples with the highest V loadings show the lowest values of E_g, which can be attributed to the dominant role of larger crystallites of $Mg_3V_2O_8$, clearly detected by XRD.

3.2. Catalytic performance of V-Mg-O catalysts in oxidative dehydrogenation of ethylbenzene

3.2.1. Effect of vanadium loading and calcination temperature

The catalytic activity of the synthesized catalysts was investigated in the oxidative dehydrogenation of EB in terms of conversion of EB and selectivity to styrene with time-on-stream at 500 °C and molar ratio of O_2:EB = 1:1 (Fig. 7A and B). The poorly active MG sample clearly improves the catalytic performance after the introduction of V phase. The initial EB conversion increases ca. 10 times (from 4.1 to 39.8%) even for the sample doped with 2 wt% of vanadium. A beneficial effect is also noticed for the selectivity to styrene (an increase from 22.7 to 76.6%). The highest initial EB conversion (63.6%) and selectivity to styrene (86.9%) were observed over the 10VMG_550 sample (Fig. 7C). The major by-product was CO_2, produced with the lowest selectivity of 11.7% in the presence of the most active 10VMG_550 sample. The cumulative selectivity to CO and benzene was lower than 2% over all samples and only traces of toluene were detected. Selectivities to particular products observed over all samples are summarized in Table S1. Such high activity found at relatively low temperature of 500 °C is promising taking into account a catalytic performance reported in the literature for V-Mg-O type catalysts, i.e. 59.1% of EB conversion with similar selectivity of 91.1% at higher temperature of 550 °C [6].

Furthermore, a discrepancy in stability between MG and the V-loaded catalysts is observed. Namely, the EB conversion and selectivity to styrene for the unmodified support grow with time-on-stream achieving a plateau, whereas for the V-containing samples the catalytic parameters decrease almost exponentially with time-on-stream. The detected variations can be explained by deposition of coke on the catalysts' surface during the ODH reaction, which is confirmed by a change of color from yellowish to dark gray and an increase in the catalyst mass during the reaction determined by TG analyses (Fig. 7D). According to the well-known mechanism, coke deposit is formed on ODH catalysts by condensation of styrene molecules, and under the reaction conditions is easily oxidized to create oxygen functional groups [41]. The formed carbon deposit strongly influences the catalytic activity. From one side, the coke plugs pores and covers active sites on the surface, but it can form new active sites for the ODH reaction on the other hand [42,43]. The latter effect is responsible for a slight increase in the activity of MG with time-on-stream. The EB conversion over this sample hypothetically extrapolated to t = 0 reaches a level as low as 3.3%. In this case, the carbonaceous deposit growing on the MgO surface during the catalytic reaction results in an appearance of carbonyl/quinone functional groups, which have been recognized as active sites of the ODH process [44]. Such oxygen-containing functionalities form because of the presence of oxygen in the reaction atmosphere. After ca. 4 h of time-on-stream, the catalytic activity stabilizes at the level of 5–6% of EB conversion (probably due to covering of the whole MgO surface with coke). The mechanism of ODH reaction involving active sites present in both vanadium and active-coke adjacent phases is demonstrated in Fig. 8. Individual explanations of these mechanisms are commonly accepted in the literature [45], however the coexistence of both active phases is crucial in this case.

The TG measurements showed that the carbon content deposited during the reaction is similar for MG and 2VMG_550. Therefore, the relatively small amounts of vanadium species on the 2VMG_550 surface are insignificant in terms of the rate of carbon deposit formation. If the carbon deposit (and its carbonyl/quinone groups) would be solely responsible for the possible variations in the catalytic activity, the level of EB conversion should be comparable for both of these materials, but it is not. This conclusion substantiates an extremely positive effect of

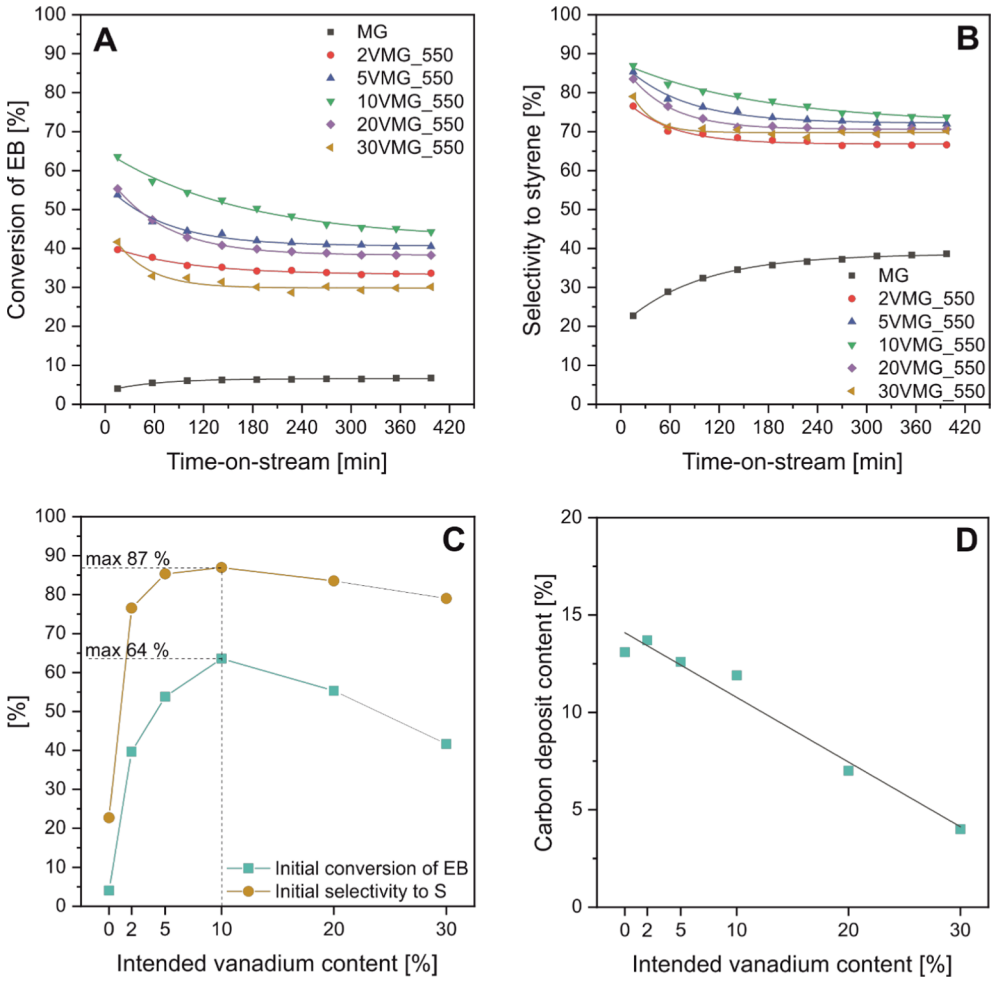

Fig. 7. Conversion of EB (A), selectivity to styrene (B), initial conversion of EB and selectivity to styrene (C), and carbon deposit content after ODH reaction (D) for the *x*VMG_550 catalysts ($T_{reaction}$ = 500 °C; O_2:EB molar ratio = 1:1).

doping with vanadium. Interestingly, the higher content of vanadium distinctly influences the extent of carbon deposit formation. The increasing vanadium loading causes a gradual decline of carbon deposit, which is aggregated in the amount as low as 4.5 wt% on the catalyst with the highest V content (cf. Fig. 7D). Such effect is related to a systematic decrease in the relative area of uncoated MgO support by the formed vanadium-containing domains. Evidently, the formation of carbon deposit is less feasible on the vanadium species, hence this process has moderately selective character and goes faster on the MgO surface.

The postulated mechanism of the ODH reaction on V-Mg-O catalysts involves two VO_4 forms as active sites, where two hydroxyl groups are created on oxygen atoms during the dehydrogenation reaction, with simultaneous reduction of vanadium sites ($V^{5+} \rightarrow V^{4+}$) [7,46,47]. A low amount of superficial vanadium species impedes detaching of both hydrogen atoms from the ethyl group of EB molecule. Distances between them are too large. On the other hand, a high V amount and forming of polymeric forms of magnesium orthovanadate lead to substantial coverage of the support with a multilayer of mixed oxide. Consequently, such aggregates act as pure $Mg_3V_2O_8$, which exhibits much lower catalytic activity in ODH than MgO-supported catalysts [9]. In the case of the developed catalysts, the optimum content of vanadium was found for the 10VMG_550 sample, which exhibits proper distances and/or sizes of VO_4 tetrahedrons clusters, promoting the

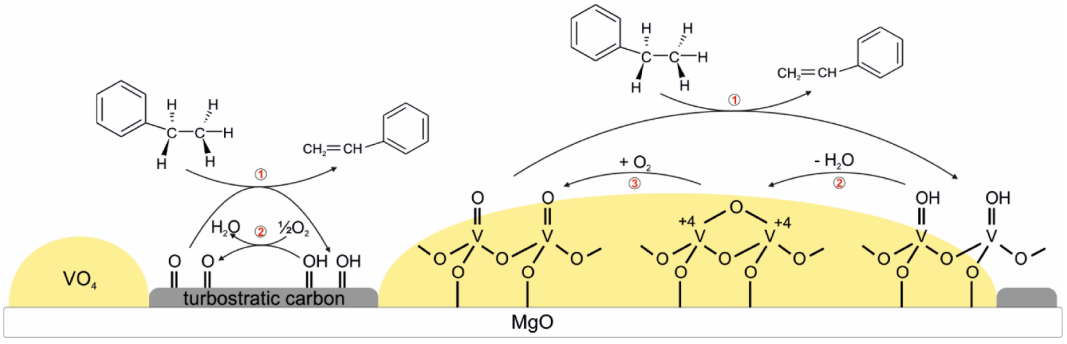

Fig. 8. Two possible mechanisms of ODH reaction on the synthesized catalysts containing a layer of deposited active coke.

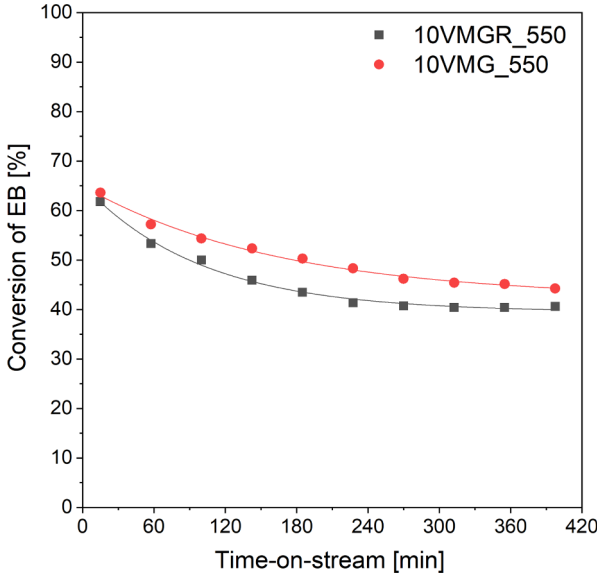

Fig. 9. Conversion of EB over 10VMG_550 and 10VMGR_550 catalysts ($T_{reaction}$ = 500 °C; O_2:EB molar ratio = 1:1).

activity in the ODH reaction. Therefore, the aggregation of such structures is inadvisable.

The catalytic activity of the reference sample (10VMGR_550) is presented in Fig. 9. The benefit of the developed mesoporous V-Mg-O system based on MG nanoreplica is clearly observed. A higher conversion of ethylbenzene is achieved over the 10VMG_550 sample compared to 10VMGR_550. Maximum relative difference observed for both catalysts reaches 16% (after ca. 180 min TOS) and decreases slightly with TOS. It is noteworthy, that the 10VMG_550 and 10VMGR_550 samples have comparable specific surface areas, i.e. 53 and 56 m^2/g, respectively. However, the total pore volume is almost two times higher for 10VMG_550 (V_{total} = 0.39 cm^3/g) than for 10VMGR_550 (0.20 cm^3/g). This variation is most likely attributed to a higher amount of micropores generated during the nanoreplication process, which can be responsible for the enhanced catalytic activity. These results confirm the positive catalytic effect of spatial structure of the 10VMG_550 catalyst.

In order to investigate the influence of calcination temperature on the catalytic activity, the sample with optimal 10 wt% of vanadium, but calcined at 800 °C was also tested (Fig. 10A and B). As can be seen, the 10VMG_550 sample exhibits much higher catalytic activity than the analogous sample annealed at 800 °C. The maximum difference in the EB conversion is noticed after 60 min of time-on-stream. This catalytic

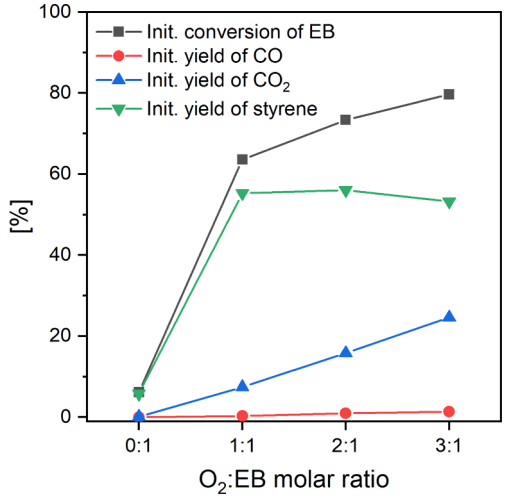

Fig. 11. Initial conversion of EB and initial yields of CO, CO_2 and styrene at various O_2:EB molar ratios ($T_{reaction}$ = 500 °C).

parameter is more than two times greater for the sample calcined at 550 °C. The initial EB conversion of 63.6% observed for 10VMG_550 is comparable with that achieved over commercial catalysts, which operate at temperatures ca. 100 °C higher, but at slightly lower selectivity to styrene of 86.9%. The differences in the catalytic activity observed for 10VMG_550 and 10VMG_800 are most likely related to size of crystallites of active phase (compare the XRD results shown in Fig. 3A). The formation of 3D $Mg_3V_2O_8$ crystallites after the thermal treatment at 800 °C results in non-optimal distribution of tetrahedral VO_4 active sites compared to less crystalline systems formed by heating at 550 °C.

3.2.2. *Influence of oxidizing agent concentration*

Assuming sensitivity of the carbon deposit formation on the concentration of oxidizing agent, we decided to investigate the behavior of the 10VMG_550 sample in the ODH reaction performed at varying O_2 contents – the O_2:EB molar ratio was changed from 0:1 (without oxygen) through 1:1 and 2:1 to 3:1 (with an excess of oxygen). The initial catalytic parameters are shown in Fig. 11. Obviously, the influence of oxygen on the catalytic performance is outstanding. In the absence of the oxidizing agent the initial EB conversion is as low as 6.2%, whereas at the lowest O_2:EB molar ratio of 1:1, this parameter increases up to ca. 63.6%. The increase in the oxygen concentration (O_2:EB molar ratios of 2:1 and 3:1) results in a further growth of initial EB conversion reaching even 79.7%. However, above equimolar O_2:EB ratio, the initial yield of styrene is negatively correlated with this parameter. This

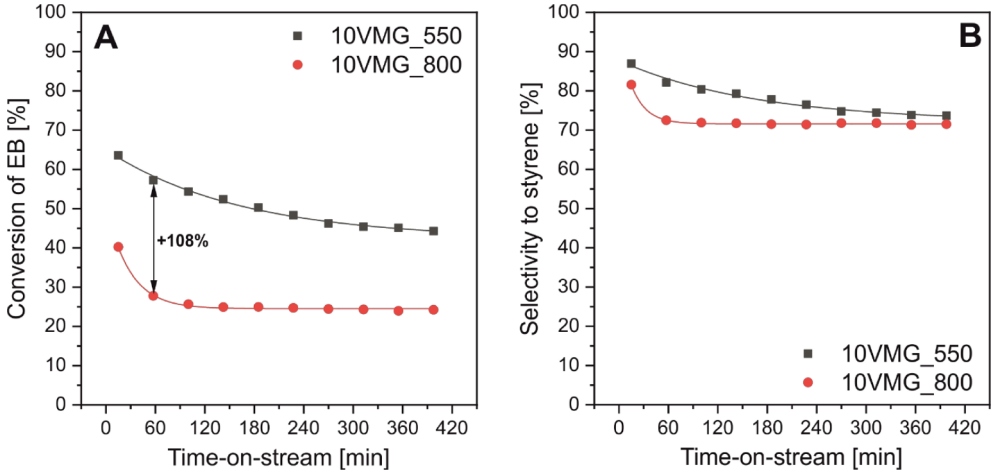

Fig. 10. Conversion of EB (A) and selectivity to styrene (B) for 10VMG_550 and 10VMG_800 catalysts ($T_{reaction}$ = 500 °C; O_2:EB molar ratio = 1:1).

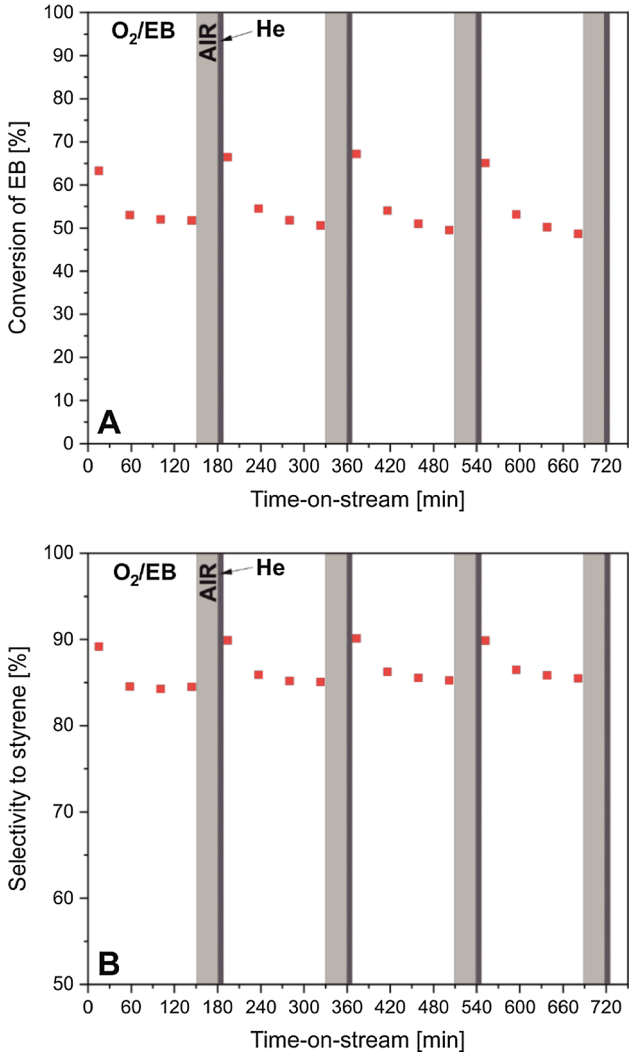

Fig. 12. Conversion of EB (A) and selectivity to styrene (B) for 10VMG_550 in four consecutive regeneration cycles performed in air ($T_{reaction}$ = 500 °C; O_2:EB molar ratio = 1:1).

observation is in agreement with a simultaneous increase in the initial yield of CO_2. The oxygen-rich reaction atmosphere accelerates deeper oxidation of EB, and as a consequence, lower yields of styrene are achieved. The O_2:EB molar ratio of 1:1 is in that case optimal in terms of the best catalytic activity in the ODH reaction for the catalyst containing 10 wt% of vanadium in the form of VO_4 active sites highly dispersed on the surface of magnesium oxide support.

3.2.3. Catalyst regeneration

The substantial impact of carbon deposit on the catalytic activity found for all examined samples stimulated us to study the possibility of regeneration of the developed V-Mg-O catalysts. For the most active 10VMG_550 material, a series of four cycles including catalytic tests and regeneration periods in air were performed (Fig. 12A and B). The proposed simple regeneration procedure resulted in almost complete restoration of catalytic activity after relatively short time of 30 min. Moreover, this effect is reproducible. In each of four regeneration cycles, the conversion of EB and selectivity to styrene are at the level of fresh catalyst, where relatively fast stabilization is observed. A slightly faster deactivation is noticed in the conversion of EB. Moreover, the initial conversion of ethylbenzene after each regeneration cycle is slightly higher than for a fresh catalyst.

In order to investigate the above described effects, the spent

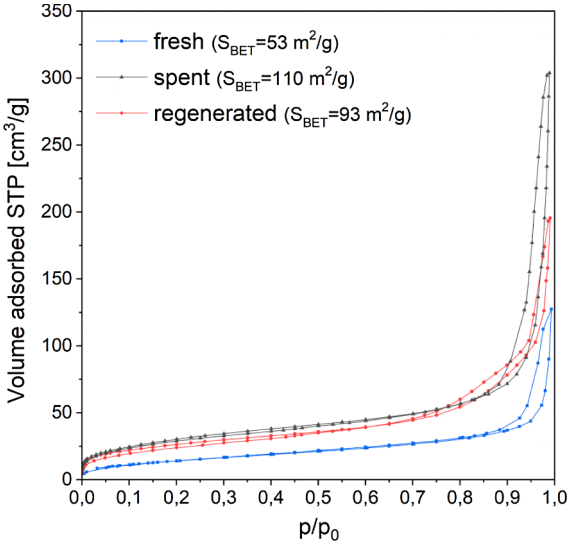

Fig. 13. Low-temperature nitrogen adsorption-desorption isotherms for the fresh, spent and regenerated 10VMG_550 catalyst.

10VMG_550 catalyst (the sample obtained after four hours of the ODH reaction, subsequent regeneration and next 4 h of the reaction) as well as the sample after fourth regeneration step were analyzed with low-temperature N_2 adsorption/desorption, TG and XPS. The collected isotherms are depicted together with the calculated specific surface areas in Fig. 13. The volume of adsorbed N_2 for the spent catalyst is greater than for the fresh one. The value of S_{BET} increases during the ODH reaction two times (from 53 m^2/g up to 110 m^2/g), most probably due to porosity of the deposited coke. A dark brown color of the spent catalyst as well as the results of TG analysis (8.0 wt% of coke detected) support this conclusion. Interestingly, the regenerated catalyst presents different properties than the fresh sample. A light gray color of that sample indicates that some coke still remains after regeneration (5 wt% as shown by TG). The presence of carbon deposit results in an enhanced porosity of this material, which is only slightly lower than the spent catalyst. The type of isotherms recorded for the fresh and regenerated catalysts are comparable. They differ only in terms of an amount of adsorbed nitrogen, which indicates no significant changes in pore arrangement during the regeneration process. Even though the carbon deposit was not removed completely, the initial catalytic activity of the regenerated catalyst is comparable with the fresh material. That corresponds well with the proposed mechanism of the ODH reaction involving both carbon deposit and vanadium containing species (cf. Fig. 8). The XPS C 1s spectra (Fig. 14) collected for the fresh, spent and regenerated 10VMG_550 catalyst confirm the differences in the amount and kind of carbon moieties present on the external surface. The fresh sample exhibits four photoemission peaks at 284.6 eV (C−C and C═C), 286.3 eV (C−OH), 288.3 eV (C═O) and 289.8 eV (carbonates), which originate from adsorbed carbon-containing species. It is observed, that during the ODH reaction carbonates disappear entirely, and partially oxidized coke is formed. Its amount decreases significantly on the surface of 10VMG_550 after regeneration. The analysis of V $2p_{3/2}$ photoelectron peaks collected for the fresh (Fig. 4) and regenerated (Fig. S8) 10VMG_550 catalysts indicates, that the oxidation state of vanadium did not change during the regeneration process. The binding energy of symmetric photoelectron peak is equal to 517.2 eV, thus nearly identical to the fresh sample (517.1 eV).

Such regeneration of the vanadium-containing catalysts supported on mesoporous magnesia replica has not been reported yet and is promising in terms of possible application of this kind of catalytic system.

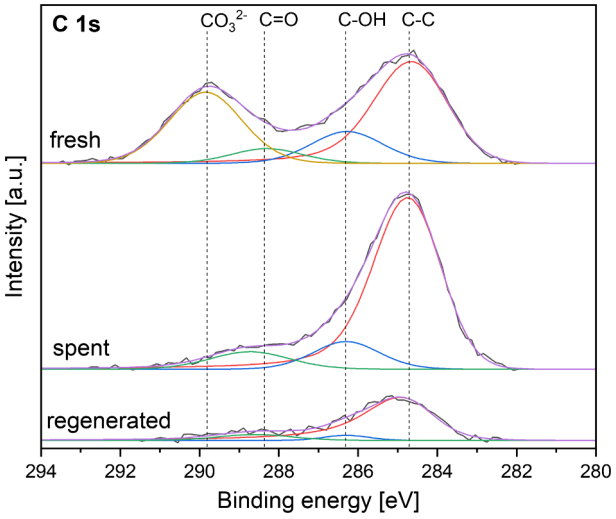

Fig. 14. XPS C 1s spectra collected for the fresh, spent and regenerated 10VMG_550 catalyst.

4. Conclusions

Mesoporous V-Mg-O catalysts with various vanadium loadings were synthesized by nanoreplication of CMK-3 rigid carbon template and subsequent wet impregnation using NH_4VO_3 as the vanadium precursor. After the thermal treatment at elevated temperatures the catalysts containing VO_x species distributed on the surface of MgO were obtained. The characterization techniques (including XRD, low-temperature N_2 adsorption, TEM, H_2-TPR, XPD and UV–Vis-DR spectroscopy) revealed that at low V contents, mainly isolated VO_4 species and small clusters of VO_x appeared. The increasing V loading resulted in aggregation of these structures towards 3D $Mg_3V_2O_8$ crystallites, which were preferably formed under the synthesis conditions.

The collected results showed, that three main factors influence the catalytic activity of the produced materials in the oxidative dehydrogenation of ethylbenzene, i.e. surface concentration of isolated VO_4 species, oxygen concentration in the reaction gas mixture, which should be optimized for a particular V-Mg-O catalytic system, and coke deposition. In the presented study, the vanadium concentration of 10 wt% and the O_2:EB molar ratio equal to 1:1 turned out to be optimal, resulting in the conversion of EB of 63.6% at the selectivity to styrene of 86.9% at the reaction temperature as low as 500 °C. The coke deposit contributes the overall catalytic activity, because of the presence of carbonyl/quinone ODH active sites on the carbonaceous layer. Therefore, the mechanism of the ODH reaction involving both carbon deposit and vanadium containing species was proposed. Moreover, the consecutive regeneration experiments showed, that almost complete restoration of the catalyst performance is possible after relatively short treatment in air.

Declaration of competing interest

The authors declared that there is no conflict of interest.

Acknowledgements

This work was supported by the Polish National Science Centre (grant no. 2013/09/B/ST5/03419). The research was carried out with the equipment purchased thanks to the financial support of the European Regional Development Fund in the framework of the Polish Innovation Economy Operational Program (contract no. POIG.02.01.00-12-023/08). S.J. received a doctoral scholarship from the Polish National Science Centre (grant no. 2016/20/T/ST5/00256). J.S.A. acknowledges financial support by MINECO (Project MAT2016-80285-p), H2020 (MSCA-RISE-2016/NanoMed Project), and GV (PROMETEOII/2014/004).

Appendix A. Supplementary material

Supplementary data to this article can be found online at https://doi.org/10.1016/j.apsusc.2019.144336.

References

[1] I. Rossetti, E. Bencini, L. Trentini, L. Forni, Study of the deactivation of a commercial catalyst for ethylbenzene dehydrogenation to styrene, Appl. Catal. A 292 (2005) 123–188.
[2] F. Cavani, F. Trifirò, Alternative processes for the production of styrene, Appl. Catal. A 133 (1995) 219–239.
[3] K. Weissermel, H.-J. Arpe, Industrial Organic Chemistry, John Wiley & Sons Ltd. (2008) 109.
[4] A. Sun, Z. Qin, S. Chen, J. Wang, Ethylbenzene dehydrogenation in the presence of carbon dioxide over alumina supported catalysts, Catal. Today 93–95 (2004) 273–279.
[5] S. Chen, Z. Qin, G. Wang, M. Dong, J. Wang, Promoting effect of carbon dioxide on the dehydrogenation of ethylbenzene over silica-supported vanadium catalysts, Fuel 109 (2013) 43–48.
[6] J. Sakurai, T. Suzaki, K. Nakagawa, N. Ikenaga, H. Aota, T. Suzuki, Dehydrogenation of ethylbenzene over vanadium oxide-loaded MgO catalyst: promoting effect of carbon dioxide, J. Catal. 209 (2002) 16–24.
[7] J. Hanuza, W. Oganowski, Structure of the active layer and catalytic mechanism of the V_2O_5/MgO catalysts in the oxidative dehydrogenation of ethylbenzene to styrene, J. Mol. Catal. 29 (1985) 109–143.
[8] I. Kainthla, J.T. Bhanushali, R.S. Keri, B.M. Nagaraja, Activity studies of vanadium, iron, carbon and mixed oxides based catalysts for the oxidative dehydrogenation of ethylbenzene to styrene: a review, Catal. Sci. Technol. 5 (2015) 5062–5076.
[9] W. Oganowski, J. Hanuza, L. Kępiński, W. Mišta, M. Mączka, A. Wyrostek, Z. Bukowski, New intermediate phases in formation at V-Mg–O catalyst, J. Mol. Catal. A: Chem. 136 (1998) 91–104.
[10] W. Oganowski, J. Hanuza, L. Kępiński, Catalytic properties of $Mg_3(VO_4)_2$-MgO system in oxidative dehydrogenation of ethylbenzene, Appl. Catal. A 171 (1998) 145–154.
[11] N.M. Julkapli, S. Bagheri, Magnesium oxide as a heterogeneous catalyst support, Rev. Inorg. Chem. 36 (1) (2015) 1–41.
[12] M.F.R. Pereira, J.J.M. Órfão, J.L. Figueiredo, Influence of the textural properties of an activated carbon catalyst on the oxidative dehydrogenation of ethylbenzene, Colloids Surf. A 241 (2004) 165–171.
[13] J. Roggenbuck, M. Tiemann, Ordered mesoporous magnesium oxide with high thermal stability synthesized by exotemplating using CMK-3 carbon, J. Am. Chem. Soc. 127 (2005) 1096–1097.
[14] S. Jarczewski, M. Drozdek, P. Michorczyk, C. Cuadrado-Collados, J. Gandara-Loe, J. Silvestre-Albero, P. Kuśtrowski, Oxidative dehydrogenation of ethylbenzene over CMK-1 and CMK-3 carbon replicas with various mesopore architectures, Microporous Mesoporous Mater. 271 (2018) 262–272.
[15] PDF-4+ 2018; ICDD: Newtown Square, PA, 2018; PDF 00-004-0829, PDF 00-037-0351, PDF 00-041-1426.
[16] M. Thommes, K. Kaneko, A.V. Neimark, J.P. Olivier, F. Rodríguez-Reinoso, J. Rouquerol, K.S.W. Sing, Physisorption of gases, with special reference to the evaluation of surface area and pore size distribution (IUPAC Technical Report), Pure Appl. Chem. 87 (2015) 1051–1069.
[17] E.F. Aboelfetoh, M. Fechtelkord, R. Pietschnig, Structure and catalytic properties of MgO-supported vanadium oxide in the selective oxidation of cyclohexane, J. Mol. Catal. A: Chem. 318 (2010) 51–59.
[18] E.A. Elkhalifa, H.B. Friedrich, Oxidative dehydrogenation of *n*-octane using vanadium-magnesium oxide catalysts with different vanadium loadings, Appl. Catal. A 373 (2010) 122–131.
[19] J. Chetty, V.D.B.C. Dasireddy, S. Singh, H.B. Friedrich, The oxidative aromatization of *n*-hexane over VMgO catalysts, Reac. Kinet. Mech. Cat. 120 (2017) 307–321.
[20] B. Jonson, B. Robenstorf, R. Larrson, S.L.T. Anderson, Activity measurements and spectroscopic studies of the catalytic oxidation of toluene over silica-supported vanadium oxides, J. Chem. Soc. Faraday Trans. 84 (6) (1988) 1897–1910.
[21] J.K. Lee, U.G. Hong, Y. Yoo, Y.-J. Cho, J. Lee, H. Chang, I.K. Song, Oxidative dehydrogenation of *n*-butane over magnesium vanadate nano-catalysts supported on magnesia–zirconia: effect of vanadium content, J. Nanosci. Nanotechnol. 13 (2013) 8110–8115.
[22] S. Zhang, H. Liu, Oxidative dehydrogenation of propane over Mg-V-O oxides supported on MgO-coated silica: structural evolution and catalytic consequence, Appl. Catal. A 573 (2019) 41–48.
[23] L. Balderas-Tapia, I. Hernández-Pérez, P. Schacht, I.R. Córdova, G.G. Aguilar-Ríos, Influence of reducibility of vanadium–magnesium mixed oxides on the oxidative dehydrogenation of propane, Catal. Today 107–108 (2005) 371–376.
[24] E.F. Aboelfetoh, R. Pietschnig, Preparation, characterization and catalytic activity of MgO/SiO_2 supported vanadium oxide based catalysts, Catal. Lett. 144 (2014) 97–103.
[25] N.R. Shiju, M. Anilkumar, S.P. Gokhale, B.S. Raob, C.V.V. Satyanarayana, Oxidative dehydrogenation of ethylbenzene using nitrous oxide over vanadia–magnesia catalysts, Catal. Sci. Technol. 1 (2011) 1262–1270.

[26] S. Slyemi, S. Barama, A. Barama, J. Blanchard, H. Messaoudi, S. Casale, C. Calers, Characterization and reactivity of VMgO catalysts prepared by wet impregnation and sol–gel methods, Chem. Eng. Commun. 205 (9) (2018) 1288–1298.
[27] V.D.B.C. Dasireddy, F.B. Khan, S. Singh, H.B. Friedrich, Activation of *n*-heptane: a study with VMgO catalysts, Catal. Lett. 144 (2014) 590–597.
[28] X. Wang, H. Zhang, W. Sinkler, K.R. Poeppelmeier, L.D. Marks, Reduction of magnesium orthovanadate $Mg_3(VO_4)_2$, J. Alloys Compd. 270 (1998) 88–94.
[29] X. Gao, P. Ruiz, Q. Xin, X. Guo, B. Delmon, Effect of coexistence of magnesium vanadate phases in the selective oxidation of propane to propene, J. Catal. 148 (1994) 56–67.
[30] M.C. Biesinger, L.W.M. Lau, A.R. Gerson, R.St.C. Smart, Resolving surface chemical states in XPS analysis of first row transition metals, oxides and hydroxides: Sc, Ti, V, Cu and Zn, Appl. Surf. Sci. 257 (2010) 887–898.
[31] J.-G. Choi, The surface properties of vanadium compounds by X-ray photoelectron spectroscopy, Appl. Surf. Sci. 148 (1999) 64–72.
[32] T. Blasco, J.M. López Nieto, A. Dejoz, M.I. Vázquez, Influence of the acid-base character of supported vanadium catalysts on their catalytic properties for the oxidative dehydrogenation of *n*-butane, J. Catal. 157 (1995) 271–282.
[33] C. Pak, A.T. Bell, T.D. Tilley, Oxidative dehydrogenation of propane over vanadia-magnesia catalysts prepared by thermolysis of $OV(O^tBu)_3$ in the presence of nanocrystalline MgO, J. Catal. 206 (2002) 49–59.
[34] P. Concepción, J.M. López Nieto, J. Pérez-Pariente, Oxidative dehydrogenation of propane on VAPO-5, $V_2O_5/ALPO_4$-5 and V_2O_5/MgO catalysts. Nature of selective sites, J. Mol. Catal. A: Chem. 99 (1995) 173–182.
[35] F. Arena, F. Frusteri, A. Parmaliana, Structure and dispersion of supported-vanadia catalysts. Influence of the oxide carrier, Appl. Catal. A 176 (1999) 189–199.
[36] T. Crispim da Silva, E.B. Pereira, R. Pereira dos Santos, B. Louis, J.-P. Tessonnier, M.M. Pereira, Synthesis and characterization of vanadium species coated on alumina, magnesium oxide and hydrotalcite supports to SO_x removal, Appl. Catal. A 462–463 (2013) 46–55.
[37] R.S. Weber, Effect of local structure on the UV-visible absorption edges of molybdenum oxide clusters and supported molybdenum oxides, J. Catal. 151 (1995) 470–474.
[38] A.M. de Aguilar Cruz, J.G. Eon, Boehmite-supported vanadium oxide catalysts, Appl. Catal. A 167 (1998) 203–213.
[39] X. Gao, S.R. Bare, B.M. Weckhuysen, I.E. Wachs, In situ spectroscopic investigation of molecular structures of highly dispersed vanadium oxide on silica under various conditions, J. Phys. Chem. B 102 (1998) 10842–10852.
[40] J. Scholz, A. Walter, T. Ressler, Influence of MgO-modified SBA-15 on the structure and catalytic activity of supported vanadium oxide catalysts, J. Catal. 309 (2014) 105–114.
[41] G. Emig, H. Hofmann, Action of zirconium phosphate as a catalyst for the oxydehydrogenation of ethylbenzene to styrene, J. Catal. 84 (1983) 15–26.
[42] C.H. Collet, J. McGregor, Things go better with coke: the beneficial role of carbonaceous deposits in heterogeneous catalysis, Catal. Sci. Technol. 6 (2016) 363–378.
[43] V. Zarubina, C. Nederlof, B. van der Linden, F. Kapteijn, H.J. Heeres, M. Makkee, I. Melián-Cabrera, Making coke a more efficient catalyst in the oxidative dehydrogenation of ethylbenzene using wide-poretransitional aluminas, J. Mol. Catal. A: Chem. 381 (2014) 179–187.
[44] M.F.R. Pereira, J.J.M. Órfão, J.L. Figueiredo, Oxidative dehydrogenation of ethylbenzene on activated carbon catalysts. I. Influence of surface chemical groups, Appl. Catal. A 184 (1999) 153–160.
[45] X. Guo, W. Qi, W. Liu, P. Yan, F. Li, C. Liang, D.S. Su, Oxidative dehydrogenation on nanocarbon: revealing the catalytic mechanism using model catalysts, ACS Catal. 7 (2017) 1424–1427.
[46] K. Chen, A. Khodakov, J. Yang, A.T. Bell, E. Iglesia, Isotopic tracer and kinetic studies of oxidative dehydrogenation pathways on vanadium oxide catalysts, J. Catal. 186 (1999) 325–333.
[47] K. Chen, A.T. Bell, E. Iglesia, The relationship between the electronic and redox properties of dispersed metal oxides and their turnover rates in oxidative dehydrogenation reactions, J. Catal. 209 (2002) 35–42.